CERN-TH/2000/099 FERMILAB–PUB–00/114–T MRI-PHY-P20000304 IITK-HEP-00-02

Study of R-parity Violation at a μp Collider

Marcela Carena,[1, 2)*] Debajyoti Choudhury,[3)†] Chris Quigg,[1)‡] and Sreerup Raychaudhuri[4)§]

[1)] *Theoretical Physics Department, Fermi National Accelerator Laboratory, P.O. Box 500, Batavia, Illinois 60510 USA*

[2)] *TH Division, CERN, CH-1211 Geneva 23, Switzerland*

[3)] *Mehta Research Institute, Chhatnag Road, Jhusi, Allahabad 211 019, India*

[4)] *Department of Physics, Indian Institute of Technology, Kanpur 208 016, India*

(December 19, 2013)

Abstract

To explore the discovery possibilities of a high-energy muon-proton collider, we examine signals that could arise from direct-channel formation of supersymmetric-particle resonances through operators that do not respect R-parity.

PACS numbers: 12.60.Jv, 13.10.+q, 13.60.Hb

Typeset using REVTEX

*Email address: carena@fnal.gov

†Email address: debchou@mri.ernet.in

‡Email address: quigg@fnal.gov

§Email address: sreerup@iitk.ac.in

I. INTRODUCTION

Over the past several years, investigations into the feasibility of high-energy $\mu^+\mu^-$ colliders have raised the tantalizing prospect that it may be possible to capture enormous numbers of muons ($\gtrsim 10^{20}$ per year) and store them in intense beams [1–3]. Although much development will be required, muon colliders promise exquisite energy resolution in the few-hundred-GeV régime and may offer a path to the study of multi-TeV lepton-lepton interactions. The physics opportunities have now been explored in some detail [4–6]. The technology that would make muon colliders a reality could also be applied to the production of intense neutrino sources from stored muon beams [7] that could be exploited for studies of deeply inelastic scattering or neutrino oscillations [8].

If an energetic muon beam is stored in proximity to a high-energy proton beam, it is natural to consider the possibility of bringing them into collision. A luminosity of 10^{32} – 10^{33} cm^{-2}s^{-1} might be achieved in collisions of a stored $\mu^\pm$ beam with the 1-TeV proton beam of the Fermilab Tevatron [9]. With a 200-GeV muon beam, such a machine would have an impressive kinematic reach, with $\sqrt{s} \approx 0.9$ TeV and $Q^2_{\rm max} \approx 8 \times 10^5$ GeV^2. For comparison, DESY's $e^\pm p$ collider HERA has operated recently with 27.5-GeV electrons on 920-GeV protons, for $\sqrt{s} \approx 0.32$ TeV and $Q^2_{\rm max} \approx 10^5$ GeV^2. The lifetime integrated luminosity of HERA is projected as 1 fb^{-1}.

Because of the high luminosity and the large kinematic reach, physics at high Q^2 is potentially very rich [10,11]. In one year of high-luminosity operation (*i.e.*, at 10 fb^{-1}), the μp collider would yield about a million charged-current $\mu^- p \to \nu_\mu +$ anything events with $Q^2 > 5000$ GeV^2. For comparison, the H1 detector at HERA has until now recorded about 360 such $e^\pm p$ charged-current events, and can expect about 6800 over HERA's lifetime [12]. The search for new phenomena, including leptoquarks and squarks produced in R-parity–violating interactions, would be greatly extended [13].

To quantify the discovery reach of a μp collider, we explore supersymmetric processes mediated by R-parity-violating interactions in $\mu^\pm p$ collisions. We find that direct-channel formation of squarks through $\not{R}$ couplings with ordinary particles can produce sharp peaks in the invariant-mass distribution and dramatic enhancements in the Q^2 distribution. The search for these effects has the potential to significantly increase experimental sensitivity to $\not{R}$ couplings. This work complements an earlier study of the manifestations of R-parity violation in ultrahigh-energy neutrino interactions [14].

II. R-PARITY AND SUPERSYMMETRY

Electroweak gauge invariance forbids terms in the standard-model Lagrangian that change either baryon number or lepton number. Such terms are allowed in the most general supersymmetric (SUSY) extension of the standard model [15], but they may lead to an unacceptably short proton lifetime. One way to evade the proton-decay problem is to impose a discrete symmetry called R-parity, which implies a conserved multiplicative quantum number, $R \equiv (-1)^{3B+L+2S}$, where B is baryon number, L is lepton number, and S is spin [16]. All ordinary particles are R-parity even, while all superpartners are R-parity

odd. If R-parity is conserved, superpartners must be produced in pairs and the lightest superpartner, or LSP, is absolutely stable.

Imposing R-parity invariance on the SUSY Lagrangian is an *ad hoc* remedy not derived from any known fundamental principle. For this reason alone, it is of interest to consider an R-parity–violating extension of the minimal supersymmetric standard model.

The most general $\not{R}$ terms in the superpotential consistent with Lorentz invariance, gauge symmetry, and supersymmetry are[1]

$$W_{\not{R}} = \lambda_{ijk} L^i L^j \bar{E}^k + \lambda'_{ijk} L^i Q^j \bar{D}^k + \lambda''_{ijk} \bar{U}^i \bar{D}^j \bar{D}^k \tag{2.1}$$

where i, j, k are generation indices, $L^i \ni (\nu^i, e^i)_{\rm L}$ and $Q^i \ni (u^i, d^i)_{\rm L}$ are the left-chiral superfields, and $E^i \ni e^i_{\rm R}$, $D^i \ni d^i_{\rm R}$, and $U^i \ni u^i_{\rm R}$ are the right-chiral superfields, respectively. The Yukawa couplings λ_{ijk}, λ'_{ijk}, and λ''_{ijk} are *a priori* arbitrary, so the $\not{R}$ superpotential (2.1) introduces 45 free parameters.

The LLE and LQD terms change lepton number, whereas the UDD term changes baryon number. Since we wish to explore $\not{R}$ effects in μp collisions, we shall explicitly forbid the UDD interactions [19] as the most economical way to avoid unacceptably rapid proton decay. When we expand the superfield components in (2.1), we obtain the interaction Lagrangian that contributes to $\mu^{\pm} p$ interactions,

$$\mathcal{L}_{LQD} = \lambda'_{ijk} \left\{ \tilde{\nu}^i_{\rm L} d^j_{\rm L} \bar{d}^k_{\rm R} - \tilde{e}^i_{\rm L} u^j_{\rm L} \bar{d}^k_{\rm R} + \tilde{d}^j_{\rm L} \nu^i_{\rm L} \bar{d}^k_{\rm R} - \tilde{u}^j_{\rm L} e^i_{\rm L} \bar{d}^k_{\rm R} + \tilde{d}^{kc}_{\rm R} \nu^i_{\rm L} d^j_{\rm L} - \tilde{d}^{kc}_{\rm R} e^i_{\rm L} u^j_{\rm L} \right\} + \text{H.c.} \tag{2.2}$$

The $\not{R}$ couplings in (2.2) modify supersymmetric phenomenology in several important ways: processes that change lepton number are allowed, superpartners can be produced singly, and the LSP—now unstable against decay into ordinary particles—is no longer constrained by potential cosmological embarrassments to be a neutral color singlet.

The remarkable agreement between present data and standard-model (SM) expectations implies very restrictive bounds on the strength of many $\not{R}$ operators [20–24]. Experimental limits on LQD couplings of muons with the first-generation quarks found in nucleon targets are not terribly restrictive. Muon couplings to second- and third-generation quarks are still less constrained. In Table I, we summarize the constraints on the $\not{R}$ Yukawa couplings that are relevant for $\mu^{\pm} p$ collisions, for the case of a 200-GeV/c^2 sfermion. In each example we consider, we shall assume that only one $\not{R}$ coupling can be sizeable at a time [25].

R-parity–violating interactions have been looked for in many experiments. At the Tevatron Collider, for example, squark pair production and subsequent decays through an $\not{R}$ coupling could lead to an excess of events with a dilepton pair along with jets [26]. More interestingly, (Majorana) gluinos can decay through both squarks and antisquarks to produce like-sign dileptons [27]. Until superpartners are discovered, all such analyses, of necessity, rest on *ad hoc* assumptions about the spectrum. Moreover, they cannot determine the *strength* of the $\not{R}$ coupling. The last criticism does not apply to the HERA experiments [28] or to Drell-Yan processes at the Tevatron Collider [29].

---

[1]We suppress here the $\mathrm{SU}(2)_{\rm L}$ and $\mathrm{SU}(3)_c$ indices. Symmetry under $\mathrm{SU}(2)_{\rm L}$ implies that the first term is antisymmetric under $i \leftrightarrow j$, while $\mathrm{SU}(3)_c$ symmetry dictates that the third term is antisymmetric under $j \leftrightarrow k$. We neglect bilinear terms that mix lepton and Higgs superfields [17]. Discussions of the phenomenological implications of such terms can be found in the literature [18].

III. R-PARITY–VIOLATING SIGNALS AT A MUON-PROTON COLLIDER

A. General observations

The best signature for $\not{R}$ LQD couplings in μp collisions is the resonant production of a squark. If the squark decays through the same R-parity–violating coupling that produced it, this process can modify the cross section for deeply inelastic scattering. If the squark also decays with significant probability through R-parity–conserving interactions, distinctive signals may arise from the cascade decays of the squark through gaugino channels. In this article we analyze in detail only the first alternative, for which the signals consist of a single hard jet recoiling against a hard, isolated muon or neutrino.[2] The analysis is parallel to the case of leptoquark production and decay in μp colliders.

In $\mu^+ p$ scattering, the most important elementary process is

$$\mu^+ d \to \tilde{u}_L^j \to \mu^+ d, \tag{3.1}$$

the interaction of a μ^+ with a valence down quark through the λ'_{2j1} coupling, leading to a $\mu^+ +$ jet final state. Suppressed processes[3] involving sea quarks are

$$\mu^+ s \to \tilde{u}_L^j \to \mu^+ s, \tag{3.2}$$

through a λ'_{2j2} coupling, which leads to a $\mu^+ +$ jet final state, and

$$\mu^+ \bar{u} \to \tilde{d}_R^{kc} \to \begin{cases} \mu^+ \bar{u} \\ \bar{\nu}_\mu \bar{d} \end{cases}, \tag{3.3}$$

through a λ'_{21k} coupling, which leads with equal probability to a ($\mu^+ +$ jet) or (jet + missing energy) signature.

In $\mu^- p$ scattering, the most important elementary process is

$$\mu^- u \to \tilde{d}_R^k \to \begin{cases} \mu^- u \\ \nu_\mu d \end{cases}, \tag{3.4}$$

the interaction of a μ^- with a valence up quark through the λ'_{21k} coupling, which leads with equal probability to $\mu^- +$ jet or jet + missing energy signatures. The interactions with light sea quarks are

---

[2] A further possibility for charged-current events is the decay of a squark into a quark, which materializes as a jet, and the lightest neutralino, which subsequently decays outside the detector. This occurs naturally for a Higgsino-dominated LSP.

[3] In this section, we remark only on the resonant processes. However, all our quantitative studies include the full set of Feynman diagrams.

$$\mu^- \bar{d} \to \tilde{u}_L^{jc} \to \mu^- \bar{d} \tag{3.5}$$

through the λ'_{2j1} coupling, and

$$\mu^- \bar{s} \to \tilde{u}_L^{jc} \to \mu^- \bar{s} \tag{3.6}$$

through the λ'_{2j2} coupling. Both of these suppressed reactions lead to $\mu^- +$ jet signatures.

The largest cross sections—and the most promising signals—should arise from interactions with valence quarks, the reactions (3.1) and (3.4). We will analyze in detail the neutral-current reaction[4] $\mu^+ d \to \tilde{u}_L^j \to \mu^+ d$, and the charged-current reaction $\mu^- u \to \tilde{d}_R^k \to \nu_\mu d$. We consider muon beams of 50 and 200 GeV colliding with a 1-TeV proton beam.

A 1-TeV proton beam can be regarded as a broad-band, unseparated beam of quarks, antiquarks, and gluons, with energies typically in the range $(0, 350)$ GeV. Accordingly, the c.m. frame for collisions of valence quarks with 200-GeV muons approximately coincides with the laboratory (collider) frame. The appropriate detector is therefore symmetric, similar in concept to the current generation of general-purpose detectors at the Tevatron proton-antiproton collider, but emphasizing the detection and rejection of muons. Background from the muon halo around the muon beamline probably requires cutting out a cone of about $\pm 10^\circ$ around the beamline. The study of low-x collisions appears very difficult because of the asymmetric kinematics and the angular cutoff.

B. μp collider kinematics

The natural kinematic observables for the inclusive neutral-current reaction $\mu p \to \mu +$ anything are the energy and angle of the outgoing muon in the collider frame, E_μ and θ_μ. These quantities are not affected by hadronic fragmentation, and so distributions can be calculated reliably using parton-level Monte Carlo simulations. At high energies, where we may safely neglect the muon and proton masses, we denote the incoming proton momentum in the collider frame by

$$P = (E_p; 0, 0, E_p), \tag{3.7}$$

so that it defines the positive z-axis. The incoming muon momentum is

$$p = (E_\mu^0; 0, 0, -E_\mu^0), \tag{3.8}$$

and the outgoing muon momentum is

$$p' = (E_\mu; E_\mu \sin\theta_\mu, 0, E_\mu \cos\theta_\mu). \tag{3.9}$$

---

[4]The neutral-current reaction $\mu^- u \to \tilde{d}_R^k \to \mu^- u$ occurs with similar cross section; the valence up-quark density is roughly twice the valence down-quark density, but the $\tilde{d}_R^k$ branching fractions into $\mu^- u$ or $\nu_\mu d$ are one-half, whereas the $\tilde{u}_L^k$ branching fraction into $\mu^+ d$ is unity.

We follow the conventions evolved for the analysis of *ep* collisions at HERA, in which the angle of the outgoing charged lepton is measured with respect to the *proton* direction. The momentum transfer is defined as $q \equiv p - p'$, the square of the c.m. energy is

$$s = 2p \cdot P = 4E_\mu^0 E_p. \tag{3.10}$$

The invariant momentum transfer variable $Q^2 \equiv -q^2$ and the Bjorken scaling variables x and y can be expressed in terms of the muon energy and angle in the collider frame as

$$Q_\mu^2 = 4E_\mu^0 E_\mu \cos^2 \frac{\theta_\mu}{2} \ , \tag{3.11}$$

$$y_\mu \equiv \frac{q \cdot P}{p \cdot P} = 1 - \frac{E_\mu}{E_\mu^0} \sin^2 \frac{\theta_\mu}{2}, \tag{3.12}$$

$$x_\mu \equiv \frac{Q_\mu^2}{2q \cdot P} = \frac{Q_\mu^2}{2y_\mu p \cdot P} = \frac{Q_\mu^2}{4y_\mu E_\mu^0 E_p}. \tag{3.13}$$

Combining eqns. (3.11) and (3.12), we obtain the useful expression

$$Q_\mu^2 = \frac{(E_\mu \sin\theta_\mu)^2}{1 - y_\mu} = \frac{p_{\perp\mu}^2}{1 - y_\mu}. \tag{3.14}$$

The invariant-mass-squared of the outgoing hadronic system is

$$M_\mu^2 = x_\mu s = \frac{Q_\mu^2}{y_\mu}. \tag{3.15}$$

Following the example of the HERA terminology, we call this technique for determining the kinematic invariants the *muon method.*

For the inclusive charged-current reaction $\mu p \to \nu_\mu +$ anything, we reconstruct the kinematic invariants using a parton-level modification of the Blondel-Jacquet technique employed in *ep* experiments at HERA [30]. Let

$$p_H \equiv \sum_h (E_h, p_{xh}, p_{yh}, p_{zh}) \tag{3.16}$$

be the four-momentum of the outgoing hadronic system, summed over all hadronic clusters h. Then we may write the momentum transfer as $q = p_H - P$, whereupon

$$y_H = \frac{(p_H - P) \cdot P}{p \cdot P} = \frac{\sum_h (E_h - p_{zh})}{2E_\mu^0}. \tag{3.17}$$

Expressing (3.14) in terms of hadronic variables, we have

$$Q_H^2 = \frac{\vec{p}_{\perp H}^{\,2}}{1 - y_H} = \frac{(\sum_h \vec{p}_{\perp h})^2}{1 - y_H}, \tag{3.18}$$

where $\vec{p}_{\perp H}$ is the total transverse momentum of the hadronic flow and $\vec{p}_{\perp h}$ is the transverse momentum of hadron h. We determine x_H from the condition (3.13) and express the invariant-mass-squared of the outgoing hadronic system as

$$M_H^2 = \frac{Q_H^2}{y_H}. \tag{3.19}$$

For the parton-level simulation we present in Sec. III D, it is appropriate to use the kinematic variables of the struck parton that gives rise to the hard jet, instead of summing over hadron energies. The kinematic invariants determined by this *parton method* are then

$$y_J = \frac{E_J - p_{zJ}}{2E_\mu^0}\ , \quad Q_J^2 = \frac{\vec{p}_{\perp J}^{\,2}}{1-y_J}\ , \qquad \text{and} \qquad M_J^2 = \frac{Q_J^2}{y_J}\ . \tag{3.20}$$

In the analysis that follows, we use a parton-level Monte Carlo event generator [31] to compute tree-level cross sections. We treat the partons as observables: the struck quark is identified with a jet of the same four-momentum. The numerical results we present are based on the CTEQ4-M parton distribution functions [32]. However, we have verified that our results are not very sensitive to the exact choice of the parton distributions and hence stable under changes to other standard parametrizations.

C. Neutral-current interactions

The neutral-current reaction $\mu^+ p \to \mu^+ + \text{anything}$ is mediated by t-channel γ and Z^0 exchange in the standard electroweak theory. The inclusive cross section is given by

$$\sigma(\mu^+ p \to \mu^+ X) = \sum_q \int_0^1 \mathrm{d}x\ f_q(x,Q^2)\ \hat{\sigma}(\mu^+ q \to \mu^+ q)\ , \tag{3.21}$$

where $\hat{\sigma}(\mu^+ q \to \mu^+ q)$ is the elementary cross section for the μ^+ to scatter off quark q with momentum fraction x. The flux of quarks q in the proton is denoted by the parton distribution function $f_q(x,Q^2)$. Identifying the subprocess Mandelstam variables with those used so far (*viz.* $\hat{s} = 4xE_\mu^0 E_p$ and $\hat{t} \equiv -Q^2$), the parton-level cross sections are given by

$$\frac{\mathrm{d}\hat{\sigma}}{\mathrm{d}\hat{t}}(\mu^- + q \to \mu^- + q) = \frac{1}{16\pi\hat{s}^2}\left\{ \hat{s}^2\Big[\,|A_{LL}|^2 + |A_{RR}|^2\,\Big] + \hat{u}^2\Big[\,|A_{LR}|^2 + |A_{RL}|^2\,\Big] \right\}. \tag{3.22}$$

The helicity amplitudes A_{ab} assume very simple forms in the case of massless fermions. For example, the standard-model amplitudes can be expressed in the compact form

$$\begin{aligned}
A_{LL}^{\mathrm{SM}}(q) &= e^2 \sum_{i=\gamma,Z} \frac{L_i(\mu)L_i(q)}{\hat{t}-m_i^2} & A_{LR}^{\mathrm{SM}}(q) &= e^2 \sum_{i=\gamma,Z} \frac{L_i(\mu)R_i(q)}{\hat{t}-m_i^2} \\
A_{RL}^{\mathrm{SM}}(q) &= e^2 \sum_{i=\gamma,Z} \frac{R_i(\mu)L_i(q)}{\hat{t}-m_i^2} & A_{RR}^{\mathrm{SM}}(q) &= e^2 \sum_{i=\gamma,Z} \frac{R_i(\mu)R_i(q)}{\hat{t}-m_i^2} \\
L_\gamma(f) &= e_f & R_\gamma(f) &= e_f \\
L_Z(f) &= \frac{I_{3f} - \sin^2\theta_W e_f}{\sin\theta_W \cos\theta_W} & R_Z(f) &= -\tan\theta_W e_f
\end{aligned} \tag{3.23}$$

where e_f is the charge of the fermion and I_{3f} its weak isospin. Clearly, the amplitudes for scattering off quarks and antiquarks are related by

$$A^{\rm SM}_{aL}(\bar{q}) = -A^{\rm SM}_{aR}(q) \qquad \text{and} \qquad A^{\rm SM}_{aR}(\bar{q}) = -A^{\rm SM}_{aL}(q) \tag{3.24}$$

A similar relation obtains for μ^+ scattering. The presence of $\not{R}$ interactions can introduce either s-channel (resonance) or u-channel diagrams depending on the nature of coupling as well as the parton being scattered. A brief examination of eqns. (2.2) shows that the only amplitudes to be modified are:

$$\begin{aligned}
A_{LL}(u_j) &\longrightarrow A^{\rm SM}_{LL}(u) + \frac{\lambda'^2_{2jk}}{\hat{s} - m^2_{d_{Rk}} + i m_{d_{Rk}}\Gamma_{d_{Rk}}} \qquad & A_{LR}(\bar{u}_j) &\longrightarrow A^{\rm SM}_{LR}(\bar{u}) + \frac{\lambda'^2_{2jk}}{\hat{u} - m^2_{d_{Rk}}} \\
A_{LL}(\bar{d}_j) &\longrightarrow A^{\rm SM}_{LL}(\bar{d}) + \frac{\lambda'^2_{2kj}}{\hat{s} - m^2_{u_{Lk}} + i m_{u_{Lk}}\Gamma_{u_{Lk}}} \qquad & A_{LR}(d_j) &\longrightarrow A^{\rm SM}_{LR}(d) + \frac{\lambda'^2_{2kj}}{\hat{u} - m^2_{u_{Lk}}}
\end{aligned} \quad , \tag{3.25}$$

where $m_{q_{L,R\,k}}$ is the mass of the exchanged squark. Given equations (3.23) and (3.25), it is easy to calculate the pure standard-model contribution (the background) as well as the pure-$\not{R}$ and interference terms, which together comprise the signal. The expressions in eqn. (3.25) correspond to the case when only one of the $\not{R}$ couplings is nonzero.[5]

Before we attempt to disentangle the signal from the background, we must consider how detector characteristics may limit measurements of this specific process. Excluding a cone of half-angle 6° around the muon beam appears necessary for muon identification [10,11]. Similarly, accurate measurements involving jets that lie very close to the beam pipe seems unlikely. Thus, we shall require that

$$10^\circ < \theta_J < 170^\circ \ , \tag{3.26}$$

where θ_J is the polar angle of the struck parton in the final state (identifiable with the thrust axis of the final-state monojet), and

$$15^\circ < \theta_\mu < 165^\circ \ . \tag{3.27}$$

Such *acceptance cuts* significantly reduce the standard-model background, for it is primarily peaked in the forward direction. On the other hand, the $\not{R}$ signal due to an isotropically decaying squark resonance is much less peaked. Since a heavy squark is preferentially produced with a small momentum, the decay-product (μ and a jet) distributions are nearly isotropic.

According to the amplitudes (3.25), the only possible resonances involving a valence quark are (i) $\mu^+ + d \to \tilde{u}_{Lj}$ when λ'_{2j1} is nonzero, and (ii) $\mu^- + u \to \tilde{d}_{Rk}$ when λ'_{21k} is nonzero. For definiteness, we restrict ourselves here to the first alternative. The sensitivity

[5]For a more general case, the right-hand sides are replaced by a sum over the relevant couplings (and corresponding squark masses). We do not consider such cases in this work.

to the other channel is qualitatively similar (in fact, even somewhat greater). We show in Figure 1 the Q^2 distribution for the production of $\tilde{u}_{Lj}$ at the 200 GeV $\times$ 1 TeV machine, for several choices of parameters.

The standard-model contribution peaks at low scattering angles, or, in other words, at low Q^2 values. In contrast, the signal events typically populate a much larger Q^2 range. A look at Figure 1 thus suggests that harder Q^2 cuts would tend to enhance the signal-to-noise ratio. The presence of possible squark resonances suggests that distributions in invariant mass M_μ of the final (muon + monojet) state would be sensitive to the new physics effects. In Figure 2, we present this distribution for three different cases obtained by imposing different cuts on the minimum Q^2. As expected, the resonances stand out sharply, and are little affected by the Q^2 cut, while the background is strongly suppressed when we demand a higher Q^2 threshold.

A similar, though not so sharp, excess can also be seen in the p_T distribution shown in Figure 3. The sharp fall-off of the excess is a manifestation of the well-known Jacobian peak. The price of overzealous Q^2 cuts is to discard a large fraction of the signal in the interest of suppressing the background. For example, a cut of $Q^2 > 35,000$ GeV^2 accentuates the signal due to a 800-GeV/c^2 squark, but eliminates most of the signal due to a 200-GeV/c^2 squark (see Figure 2*c* or Figure 3*c*). The optimum value of the Q^2 cut is thus a sensitive function of the squark mass.

Rather than design a mass-specific cut, we opt to use the difference in the distributions in a slightly different, but more efficient way. We divide the Q^2–M_μ plane into equal-sized bins, and compute the number of signal ($N_n^{\mathrm{SM}+\not{R}}$) and background ($N_n^{\mathrm{SM}}$) events in each bin n for an accumulated luminosity of 1 fb^{-1}. We then define a χ^2 test of discrimination

$$\chi^2 = \sum_n \frac{\left(N_n^{\mathrm{SM}+\not{R}} - N_n^{\mathrm{SM}}\right)^2}{N_n^{\mathrm{SM}} + (\epsilon N_n^{\mathrm{SM}})^2} \tag{3.28}$$

where ϵ is a measure of the systematic error, accruing mainly from the uncertainties in luminosity measurement and parton densities. To be specific, we use a uniform grid of (4000 GeV^2, 40 GeV/c^2) and perform the sum over all the bins for which $N_n^{\mathrm{SM}} \geq 1$. For the systematic error, we choose $\epsilon = 5\%$. As it turns out, the final results are not too sensitive to the choice of ϵ.

In Figure 4, we illustrate the reach of such an experiment in the $m_{\tilde{u}_{Lj}}$-λ'_{2j1} plane. The region of the parameter space *above* the individual curves can be ruled out at the 95% C.L. Alternatively, for a given value of one of the two parameters, the corresponding projection onto the other axis gives the 98.6% C.L. limit on the other parameter. To obtain an understanding of the curves, it is instructive to consider only the resonant contribution, which goes as

$$\sigma(\mu^+ + d \to \tilde{u}_L) = \frac{\pi \lambda'^2_{2j1}}{4\pi s_{\mu p}}\, f_d\left(\frac{m^2_{\tilde{u}_L}}{s_{\mu p}}, s_{\mu p}\right) \ , \tag{3.29}$$

where f_d is the density of the d-quark at the corresponding value of the Bjorken variable $x = m^2_{\tilde{u}_L}/s_{\mu p}$ and virtuality $s_{\mu p}$. The exclusion curve obtained from this piece alone would read

$$\lambda'^2_{2j1}\,\mathcal{B}(\tilde{u}_L \to \mu^+ + d)\, f_d\left(\frac{m^2_{\tilde{u}_L}}{s_{\mu p}}, s_{\mu p}\right) = \text{constant}, \tag{3.30}$$

where $\mathcal{B}$ is the branching fraction for squark decay into the observed channel. Fixing the parton distributions, we can determine the analytic dependence of the exclusion curves on the parameters. For example, the effect of the R-conserving width Γ_R can be understood from this relation. Since the $\not{R}$ width goes as λ'^2, for small values of $\mathcal{B}$, the exclusion curve in λ' goes as $\Gamma_R^{1/4}$. With an increase in $m_{\tilde{u}_L}$, which increases the bound on λ', the $\not{R}$ width increases and becomes comparable to or even dominates over Γ_R. This, for example, leads to the coalescing of the curves for $\Gamma_R = 0.2$ GeV and $\Gamma_R = 2$ GeV (see Figure 4).

The 200 GeV $\times$ 1 TeV exclusion plot levels off at high values of $m_{\tilde{u}_L}$. For very massive squarks, resonance formation is not possible kinematically. Rather, the major effect due to the squark arises in the form of s- and u-channel exchanges that lead naturally to excesses in large Q^2, but moderate M_μ, regions of the phase space. Consequently, the dependence on the squark mass is less pronounced. In this regime, the contributions we have neglected from a right-handed squark (assumed to have a mass of 2 TeV/c^2) need to be taken into account, especially if it couples to a u-quark (λ'_{211}).

D. Charged-current interactions

The charged-current reaction $\mu^- p \to \nu_\mu + X$ is mediated by t-channel W-boson exchange and by $\tilde{d}^k_R$ excitation through the $\not{R}$ coupling λ'_{21k}. The inclusive cross section is given by

$$\sigma(\mu^- p \to \nu_\mu X) = \sum_q \int_0^1 \mathrm{d}x\; f_q(x, Q^2)\, \hat{\sigma}(\mu^- q \to \nu_\mu q')\;, \tag{3.31}$$

where $\hat{\sigma}(\mu^- q \to \nu_\mu q')$ is the elementary cross section for the μ^- to scatter off quark q with momentum fraction x. At the parton level, the only allowed charged current processes are

$$\mu^- + u_i \to \nu_\mu + d_i \qquad \text{and} \qquad \mu^- + \bar{d}_i \to \nu_\mu + \bar{u}_i \tag{3.32}$$

and the conjugate processes for a μ^+ beam. We neglect processes involving the top quark and will also neglect Cabibbo-Kobayashi-Maskawa mixing. Both approximations are excellent for the present purpose. The cross sections are much simpler than those for the neutral-current process and are given by ($\hat{t} \equiv -Q^2$)

$$\begin{aligned}
\frac{\mathrm{d}\hat{\sigma}}{\mathrm{d}\hat{t}}(\mu^- + q \to \nu_\mu + \bar{q}) &= \frac{1}{16\pi \hat{s}^2}\left|\frac{e^2}{s^2_W\,(\hat{t} - m^2_W)} + A_{\not{R}}\right|^2 \\
A_{\not{R}}(u_i) &= \frac{\lambda'^2_{2ik}}{\hat{s} - m^2_{\tilde{d}_{kR}} + i\Gamma_{\tilde{d}_{kR}} m_{\tilde{d}_{kR}}} \\
A_{\not{R}}(\bar{d}_i) &= \frac{\lambda'^2_{2ik}}{\hat{u} - m^2_{\tilde{d}_{kR}}}
\end{aligned} \tag{3.33}$$

Only a μ^- beam excites a resonance in charged-current interactions with a valence quark. The resonance contributes equally to the charged- and neutral-current processes. Furthermore, since the u-quark density in the proton is roughly twice that of the d-quark, the effect

of the smaller branching fraction is compensated to a great extent. Thus, we could have used this operation mode for the neutral-current process as well, with the difference that we would now explore a different coupling.

Because the charged-current process has no photon-exchange contribution, the forward peak of the standard-model background is significantly reduced (see Figure 5) compared to the neutral-current case. This implies that the deviation due to the presence of an $\not{R}$ coupling should be visible even at smaller Q^2 values. However, since the neutrino cannot be seen directly, we have only the relatively crude measure of Q^2_J at our disposal, so the Q^2 plateau resulting from the resonance is degraded compared with the neutral-current case.

The distributions in the resonance mass M_J reconstructed from jet variables (Figure 6), and in the jet transverse momentum p_{TJ} (Figure 7) are qualitatively similar to those for the neutral-current case. In our examples, the $\not{R}$ term interferes constructively with the standard-model background below resonance, and destructively above.

To determine the reach of this experiment, we use a similar binning as before, only now in the (Q^2_J, M_J) plane. The resultant contours are presented in Figure 8. The generic features are quite similar to those of Figure 4, but the sensitivity is greatly increased, notwithstanding the smaller number of kinematic observables. The reasons for the greater sensitivity are easy to see:

- The photon-exchange contribution, the major background in the neutral-current mode, is absent here.

- The dominant standard-model charged-current subprocess in $\mu^- p$ scattering involves the up-quark. With our choice of couplings, the dominant $\not{R}$ amplitude also involves the same quark. Thus, the interference term is maximized.

- The apparent advantage of the charged-current channel is due, in part, to our choice of the initial state. Had we considered neutral-current processes in $\mu^- p$ scattering instead, the dominant $\not{R}$ process would have been resonant production of $\tilde{d}^k_R$. The smaller branching fraction of the $\tilde{d}^k_R$ into μ^- is more than compensated by the larger flux of the u-quark. Moreover, the standard-model amplitude for $\mu^- u$ scattering being larger than that for $\mu^+ d$ scattering, the relative importance of the interference term is larger, especially for off-resonance contributions. Hence the $\mu^- p$ neutral-current exclusion curves would be slightly stronger than those displayed in Figure 4 for $\mu^+ p$.

IV. SUMMARY AND OUTLOOK

A high-energy, high-luminosity muon-proton collider would offer very interesting new possibilities to search for signals of new physics at high Q^2. To develop one example in some detail, we have examined the sensitivity of a 50- or 200-GeV (E_μ) $\times$ 1-TeV (E_p) collider to R-parity–violating couplings. We have considered situations in which only LQD $\not{R}$ couplings are nonzero. Prominent signals would arise from the resonant formation of a squark that decays into a hadron jet plus a muon or a neutrino. For a squark with mass $\lesssim 0.5$ TeV/c^2, we find that couplings $\lambda'_{2j1} \gtrsim 0.05$ and $\lambda'_{21k} \gtrsim 0.03$ could be detected at the 200-GeV $\times$ 1-TeV collider at a luminosity of 1 fb^{-1}. This represents a considerable improvement in sensitivity

over existing constraints on these couplings, as well as a significant improvement over the HERA bounds on first-generation $\not{R}$ couplings.

ACKNOWLEDGMENTS

We thank Heidi Schellman for helpful advice about angular cuts and trigger requirements. C.Q. thanks the CERN Theory Division for warm hospitality during the summers of 1998 and 1999.

Fermilab is operated by Universities Research Association, Inc., under contract DE-AC02-76CHO3000 with the United States Department of Energy.

REFERENCES

[1] The Muon Collider Collaboration, "$\mu^+\mu^-$ Collider Feasibility Study," BNL-52503 & FERMILAB–CONF–96/092, July 1996, unpublished.

[2] R. Palmer, A. Tollestrup, and A. Sessler, "Status Report of a High Luminosity Muon Collider and Future Research and Development Plans," *Snowmass '96.*

[3] R. B. Palmer for the Muon Collider Collaboration, "Muon Collider: Introduction and Status," in *Workshop on Physics at the First Muon Collider and at the Front End of the Muon Collider,* edited by S. Geer and R. Raja, AIP Conference Proceedings 435 (American Institute of Physics, Woodbury, NY, 1998), p. 11. B. Autin, A. Blondel, and J. Ellis, "Prospective Study of Muon Storage Rings at CERN," CERN 99-02, ECFA 99-197.

[4] For a very useful survey of the physics of $\mu^+\mu^-$ colliders, see V. Barger, M. S. Berger, J. F. Gunion, and Tao Han, Phys. Rep. **286,** 1 (1997).

[5] For a recent workshop summary, see C. Quigg, "Physics with a Millimole of Muons," FERMILAB–CONF–98/073–T, (electronic archive: hep–ph/9803326) in *Workshop on Physics at the First Muon Collider and at the Front End of the Muon Collider,* edited by S. Geer and R. Raja, AIP Conference Proceedings 435 (American Institute of Physics, Woodbury, NY, 1998), p. 242. See also J. F. Gunion, "Physics at a Muon Collider," UCD-98-5 (electronic archive: hep–ph/9802258), *ibid.*, p. 37.

[6] S. Geer, "Workshop on Physics at the First Muon Collider and at the Front End of the Muon Collider: a Brief Summary," in *Physics Potential and Development of $\mu^+\mu^-$ colliders ($\mu\mu$97),* edited by D. B. Cline, AIP Conference Proceedings 441 (American Institute of Physics, Woodbury, NY, 1998), p. 18. C. M. Ankenbrandt, *et al.* (Muon Collider Collaboration), "Status of Muon Collider Research and Development", Phys. Rev. ST Accel. Beams **2**, 081001 (1999), (electronic archive: physics/9901022).

[7] S. Geer, Phys. Rev. D**57,** 6989 (1998).

[8] P. Fisher and B. Kayser, "Experimental Neutrino Physics at the Muon Collider Complex, in *Workshop on Physics at the First Muon Collider and at the Front End of the Muon Collider,* edited by S. Geer and R. Raja, AIP Conference Proceedings 435 (American Institute of Physics, Woodbury, NY, 1998), p. 139; B. J. King, "Neutrino Physics at a Muon Collider," *ibid.*, p. 334; R. N. Mohapatra, "Neutrino Physics in a Muon Collider," *ibid.*, p. 358; E. A. Paschos, "Aspects of Neutrino Reactions at the First Muon Collider, *ibid.*, p. 370; D. A. Harris and K. S. McFarland, "Detectors for Neutrino Physics at the First Muon Collider," *ibid.*, p. 376; J. Yu and A. V. Kotwal, "Measurement of $\sin^2\theta_W$ at the First Muon Collider," *ibid.*, p. 398. C. Albright, *et al.*, "Physics at a Neutrino Factory," FERMILAB–FN–692 (May 9, 2000). See also the Proceedings of the ICFA/ECFA Workshop, "Neutrino Factories based on Muon Storage Rings," Lyon, 5 – 9 July 1999, to be published in Nuclear Instruments and Methods A.

[9] V. Shiltsev, "An Asymmetric Muon-Proton Collider: Luminosity Consideration," FERMILAB–CONF–97/114, presented at 17th IEEE Particle Accelerator Conference (PAC 97): Accelerator Science, Technology and Applications, Vancouver, Canada, 12-16 May 1997.

[10] H. Schellman, "Deep Inelastic Scattering at a Muon Collider – Neutrino Physics," in *Workshop on Physics at the First Muon Collider and at the Front End of the Muon*

Collider, edited by S. Geer and R. Raja, AIP Conference Proceedings 435 (American Institute of Physics, Woodbury, NY, 1998), p. 166.

[11] S. Ritz, "On Future Charged Lepton-Hadron Colliders," in *Workshop on Physics at the First Muon Collider and at the Front End of the Muon Collider,* edited by S. Geer and R. Raja, AIP Conference Proceedings 435 (American Institute of Physics, Woodbury, NY, 1998), p. 327.

[12] C. Diaconu, private communication.

[13] V. Barger, Kingman Cheung, K. Hagiwara, and D. Zeppenfeld, Phys. Rev. D**57,** 391 (1998) (electronic archive: hep–ph/9707412); Kingman Cheung, "Muon-Proton Colliders: Leptoquarks and Contact Interactions," in *Physics Potential and Development of $\mu^+\mu^-$ Colliders,* edited by D. B. Cline, AIP Conference Proceedings 441 (American Institute of Physics, Woodbury, NY, 1998), p. 338 (electronic archive: hep–ph/9802219); Kingman Cheung, "Muon-Proton Colliders: Leptoquarks, Contact Interactions, and Extra Dimensions," talk at 5th International Conference on Physics Potential and Development of Muon Colliders ($\mu\mu$99), San Francisco, California, 15-17 Dec 1999, (electronic archive: hep–ph/0001275).

[14] M. Carena, D. Choudhury, S. Lola and C. Quigg, Phys. Rev. D**58,** 095003 (1998) (electronic archive: hep–ph/9804380).

[15] For a crisp statement of the motivation for supersymmetry, see Fabio Zwirner, "Extensions of the Standard Model," in *Proc. Int. Europhys. Conf. on High Energy Physics (HEP 95),* Brussels, ed. J. Lemonne, C. Vander Velde, and F. Verbeure (World Scientific, Singapore, 1996), p. 943 (electronic archive: hep–ph/9601300).

[16] P. Fayet, Phys. Lett. **B69,** 489 (1977); G. Farrar and P. Fayet, Phys. Lett. **B76,** 575 (1978).

[17] See, *e.g.*, L. J. Hall and M. Suzuki, Nucl. Phys. **B231,** 419 (1984).

[18] M. A. Diaz, "R-parity Breaking in Minimal Supergravity," in *International Europhysics Conference on High Energy Physics,* edited by Daniel Lellouch, Giora Mikenberg, Eliezer Rabinovici (Springer-Verlag, Berlin & New York,1999), p. 895 (electronic archive: hep–ph/9712213); "The Minimal Supersymmetric Standard Model with a Bilinear R-parity Violating Term," in *Quantum Effects in the MSSM,* edited by Joan Sola (World Scientific, Singapore, 1998) p. 333 (electronic archive: hep–ph/9711435) and references therein; H. P. Nilles and N. Polonsky, Nucl. Phys. **B484,** 33 (1997); R. Hempling, *ibid.* **B478,** 3 (1996); M. Carena, S. Pokorski and C. Wagner, Phys. Lett. **B430,** 281 (1998).

[19] L. Ibañez and G. G. Ross, Phys. Lett. **B260,** 291 (1991), Nucl. Phys. **B368,** 3 (1992); S. Lola and G. G. Ross, Phys. Lett. **B314,** 336 (1993); P. Binétruy, E. Dudas, S. Lavignac and C. A. Savoy, Phys. Lett. **B422,** 171 (1998); J. Ellis, S. Lola and G. G. Ross, Nucl. Phys. **B526,** 115 (1998).

[20] V. Barger, G.F. Giudice, and T. Han, Phys. Rev. D**40,** 2987 (1989).

[21] G. Bhattacharyya and D. Choudhury, *Mod. Phys. Lett* **A10**, 1699 (1995).

[22] J. L. Goity and M. Sher, Phys. Lett. **B346,** 69 (1995); erratum: *ibid.* **B385,** 500 (1996).

[23] G. Bhattacharyya, Nucl. Phys. B (Proc. Suppl.) **52A,** 83 (1997); "A brief review of R-parity violating couplings," in *Beyond the Desert 1997: Accelerator and non-accelerator approaches,* edited by H. V. Klapdor-Kleingrothaus and H. Päs (Institute of Physics, Bristol and Philadelphia, 1998) p. 194.

[24] H. Dreiner, "An Introduction to Explicit R-parity Violation," to be published in *Per-*

spectives on Supersymmetry, edited by G. L. Kane (World Scientific, Singapore) (electronic archive: hep–ph/9707435 v2).
[25] Stringent limits on products of R-parity–violating couplings are given by K. Agashe and M. Graesser, Phys. Rev. D**54,** 4445 (1995); F. Vissani and A. Yu. Smirnov, Phys. Lett. **B380,** 317 (1996); D. Choudhury and P. Roy, Phys. Lett. **B378,** 153 (1996).
[26] B. Abbott *et al.* (D0 Collaboration), Phys. Rev. Lett. **83,** 4476 (1999), hep-ex/9907019.
[27] F. Abe *et al.* (CDF Collab.), Phys. Rev. Lett. **83,** 2133 (1999); D. Choudhury and S. Raychaudhuri, Phys. Rev. D**56,** 1778 (1997).
[28] C. Adloff *et al.* (H1 Collab). *Eur.Phys.J.* **C11** 447 (1999).
[29] G. Bhattacharyya, D. Choudhury and K. Sridhar, Phys. Lett. **B349,** 118 (1995).
[30] A. Blondel and F. Jacquet, in *Proceedings of the Study of an ep facility for Europe,* edited by U. Amaldi, DESY 79/48 (1979), p. 391.
[31] We employ the parton Monte Carlo simulation of D. Choudhury and S. Raychaudhuri, Phys. Lett. **B401,** 54 (1997).
[32] H. L. Lai, *et al.* (CTEQ Collaboration), Phys. Rev. D**55,** 1280 (1997).

TABLES

TABLE I. Experimental constraints (at one or two standard deviations) on the R-parity–violating Yukawa couplings of interest, for the case of 200 GeV/c^2 sfermions. For arbitrary sfermion mass, multiply the limits by ($m_{\tilde{f}}$/200 GeV/c^2), except for λ'_{221}.

$\not{R}$ Coupling	Limited by
$\lambda'_{21k} < 0.18$ (1σ)	π decay
$\lambda'_{221} < 0.36$ (1σ)	D decay
$\lambda'_{231} < 0.44$ (2σ)	ν_μ deep inelastic scattering

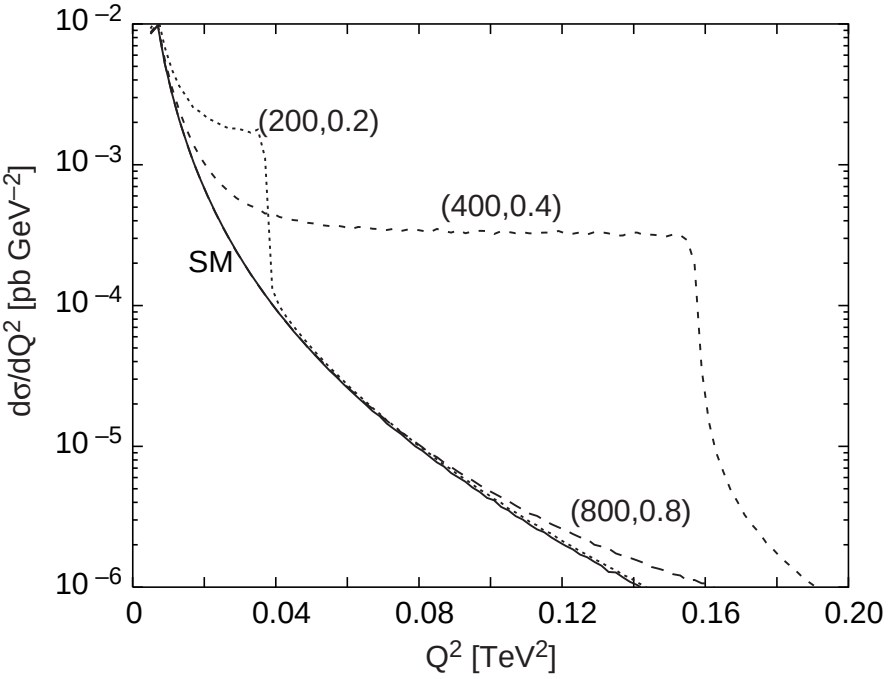

FIG. 1. The Q^2-distribution for the neutral current process $\mu^+ + p \rightarrow \mu^+ + X$ at the (200 GeV $\times$ 1 TeV) machine. The solid line represents the standard-model expectations, while the other curves are for the displayed values of $(m_{\tilde{u}_{Lj}}, \lambda'_{2j1})$. The only cuts are those of eqns. (3.26) and (3.27).

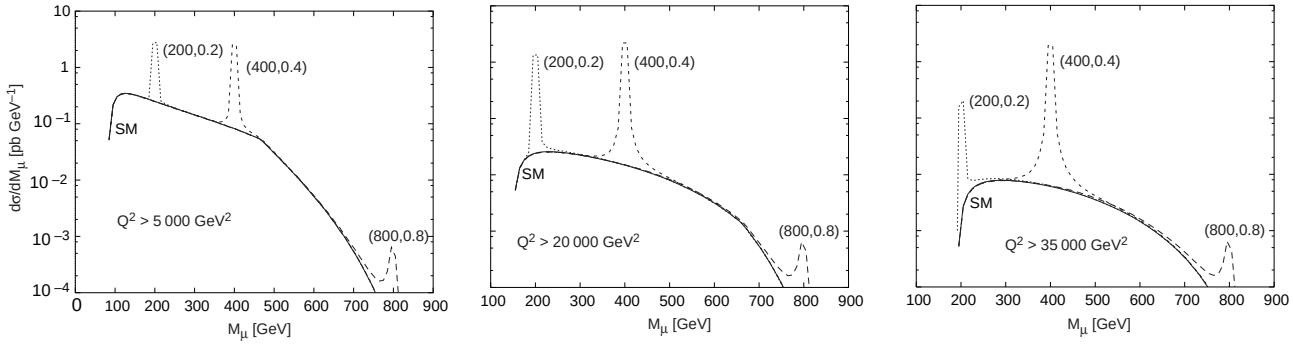

FIG. 2. The invariant mass distribution for the neutral current process $\mu^+ + p \rightarrow \mu^+ + X$ at the (200 GeV $\times$ 1 TeV) machine. The solid line represents the standard-model expectations, while the other curves are for the displayed values of $(m_{\tilde{u}_{Lj}}, \lambda'_{2j1})$. In addition to the cuts of eqns. (3.26) and (3.27), we impose a cut on Q^2.

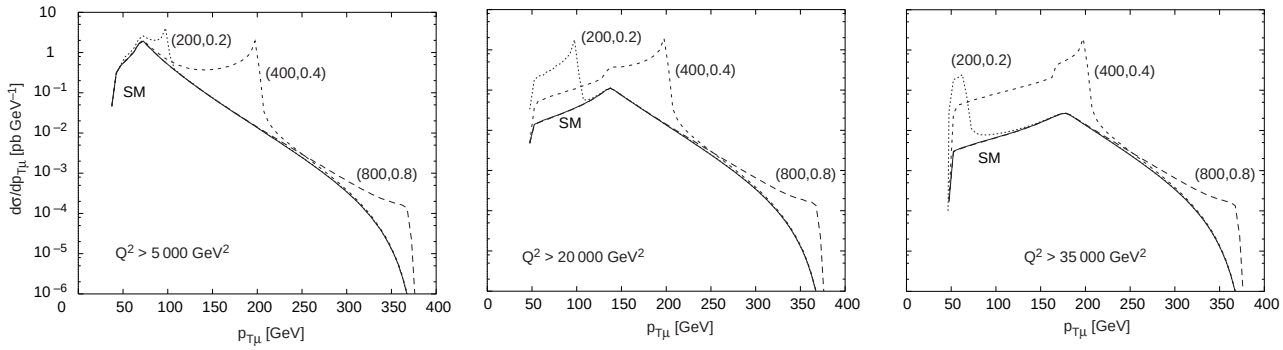

FIG. 3. The transverse momentum distribution for the neutral current process $\mu^+ + p \to \mu^+ + X$ at the (200 GeV $\times$ 1 TeV) machine. The solid line represents the standard-model expectations, while the other curves are for the displayed values of $(m_{\tilde{u}_{Lj}}, \lambda'_{2j1})$. In addition to the cuts of eqns.(3.26) and (3.27), we impose a cut on Q^2.

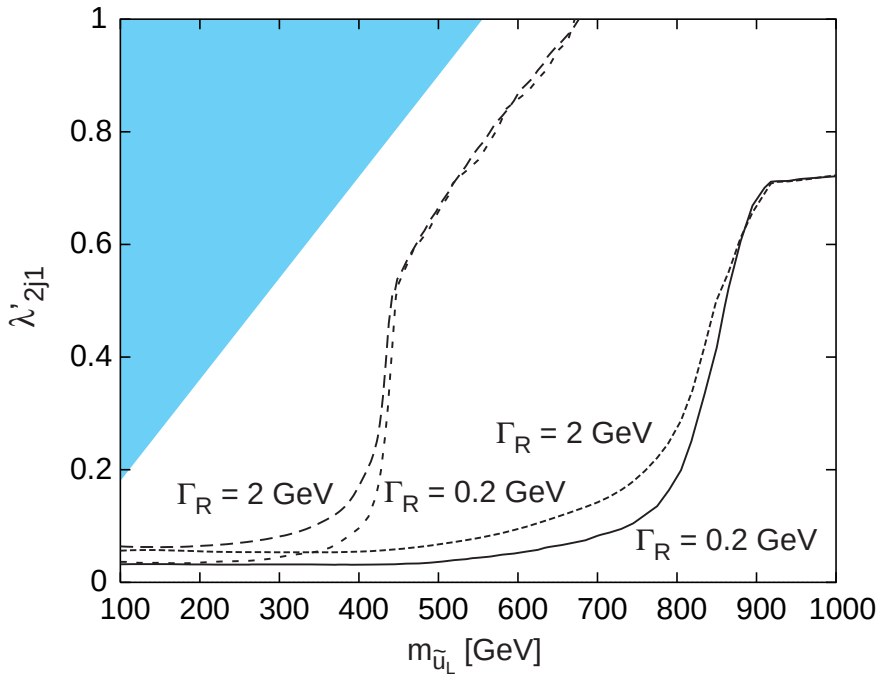

FIG. 4. Exclusion contours that may be obtained from neutral-current processes at a $\mu^+ p$ collider with an accumulated luminosity of 1 fb^{-1}. The part of the parameter space above the curves may be ruled out at the 95% C.L. The set on the left corresponds to the (50 GeV $\times$ 1 TeV) mode while that on the right corresponds to a (200 GeV $\times$ 1 TeV) machine. For each case, the dependence on the R-conserving width is also shown. The shaded region corresponds to the area ruled out by low-energy experiments. The corresponding right-handed squark is assumed to have a mass of 2 TeV/c^2.

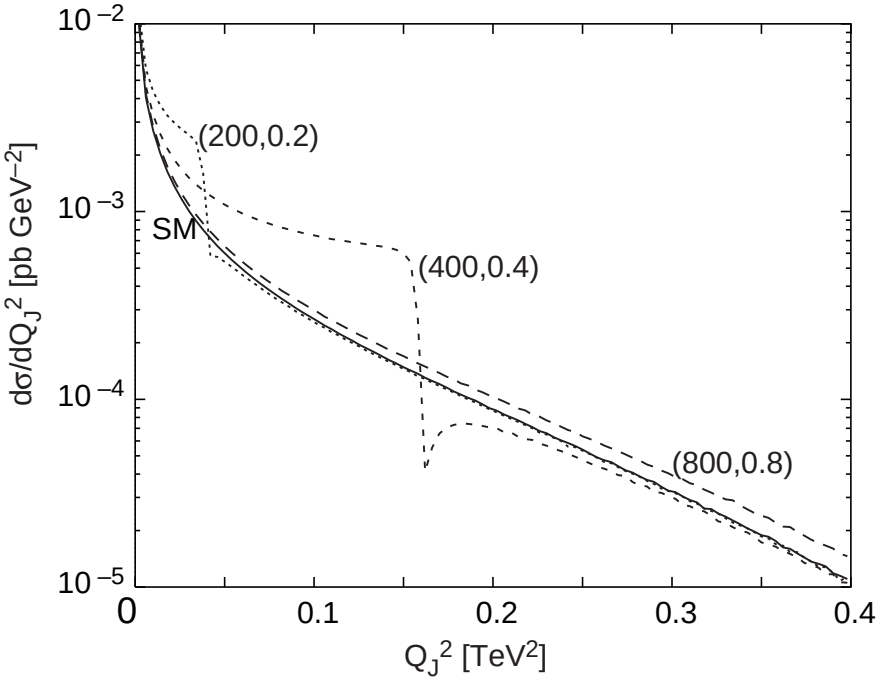

FIG. 5. The Q^2-distribution for the charged current process $\mu^- + p \to \nu_\mu + X$ at the (200 GeV $\times$ 1 TeV) machine. The solid line represents the standard-model expectations, while the other curves are for the displayed values of $(m_{\tilde{d}_{Rk}}, \lambda'_{21k})$. The only cut is that of eqn. (3.26).

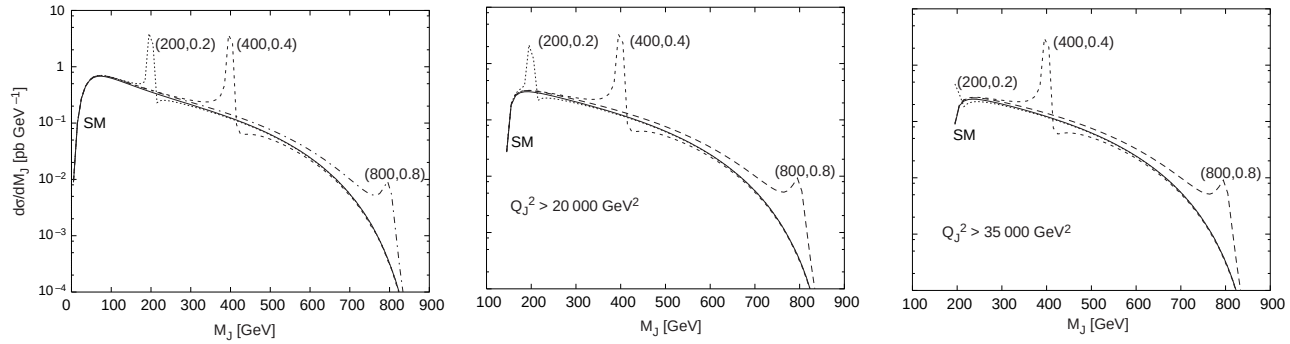

FIG. 6. The invariant mass distribution for the charged-current process $\mu^- + p \to \nu_\mu + X$ at the (200 GeV $\times$ 1 TeV) machine. The solid line represents the standard-model expectations, while the other curves are for the displayed values of $(m_{\tilde{d}_{Rk}}, \lambda'_{21k})$. In addition to the cut of eqn. (3.26), we impose a cut on Q_J^2.

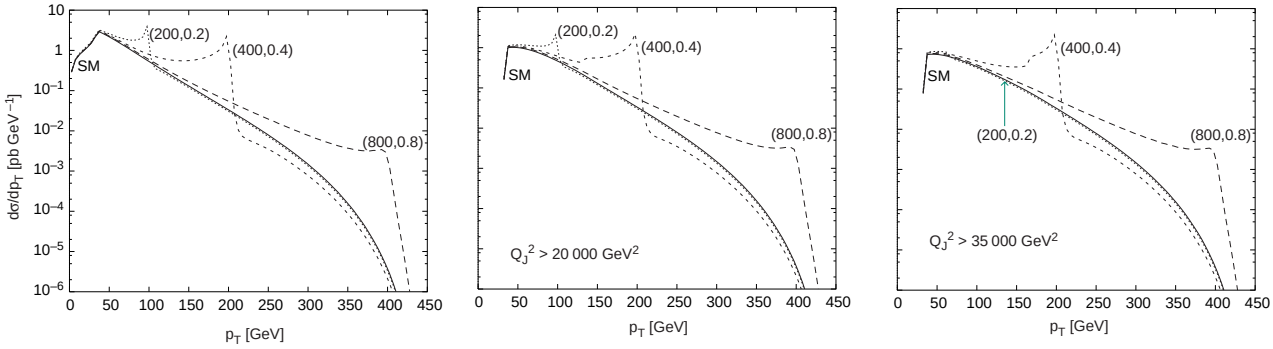

FIG. 7. The jet transverse momentum distribution for the charged-current process $\mu^- + p \to \nu_\mu + X$ at the (200 GeV $\times$ 1 TeV) machine. The solid line represents the standard-model expectations, while the other curves are for the displayed values of $(m_{\tilde{d}_{Rk}}, \lambda'_{21k})$. In addition to the cut of eqn. (3.26), we impose a cut on Q_J^2.

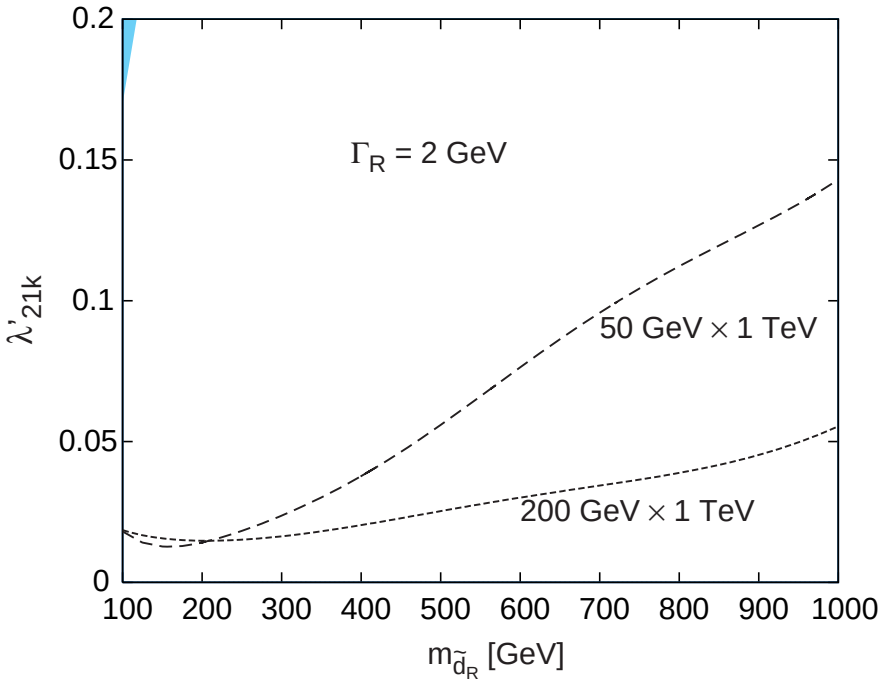

FIG. 8. Exclusion contours that may be obtained from the charged-current process at a $\mu^- p$ collider with an accumulated luminosity of 1 fb^{-1}. The part of the parameter space above the curves may be ruled out at 95% C.L. The tiny shaded region in the northwest corner corresponds to the area ruled out by low-energy experiments. The corresponding left-handed squarks are assumed to have a mass of 2 TeV/c^2.